

## Article

# Influence of Teleconnection Factors on Extreme Precipitation in Henan Province under Urbanization

Yuxiang Zhao <sup>1,2</sup>, Jie Tao <sup>1,2</sup>, He Li <sup>1,2,\*</sup>, Qiting Zuo <sup>1,2</sup> , Yinxing He <sup>3</sup> and Weibing Du <sup>4</sup>

<sup>1</sup> School of Water Conservancy and Transportation, Zhengzhou University, Zhengzhou 450001, China; zhaoyuxiang1998@126.com (Y.Z.); taojie2015@zzu.edu.cn (J.T.); zuoqt@zzu.edu.cn (Q.Z.)

<sup>2</sup> Yellow River Ecological Protection and Regional Coordinated Development Research Institute, Zhengzhou University, Zhengzhou 450001, China

<sup>3</sup> Water Conservancy Security Center of East Henan, Kaifeng 475000, China

<sup>4</sup> Henan Water Diversion Engineering Co., Ltd., Zhengzhou 450003, China

\* Correspondence: lihe@zzu.edu.cn

**Abstract:** Urban extreme precipitation is a typical destructive hydrological event. However, the disaster-causing factors of urban extreme precipitation in Henan Province have rarely been discussed. In this study, daily precipitation data of 11 stations covering a disaster-affected area in “21.7” rainstorm event from 1951 to 2021 and hundreds of climatic indexes set were selected. First, the Granger causality test was adopted to identify the dominant teleconnection factors of extreme precipitation. Then, the effects of teleconnection factors on extreme precipitation in four design frequencies of 10%, 1%, 0.1%, and 0.001% in typical cities of Henan Province were analyzed by using regression and frequency analysis. Finally, the future variation was predicted based on CMIP6. The results show that: (1) The West Pacific 850 mb Trade Wind Index, Antarctic oscillation index, and other factors exert common influence on disaster-affected cities. (2) Teleconnection factors are the dominant force of urban extreme precipitation in most cities (50.3–99.8%), and area of built-up districts, length of roads, area of roads, and botanical garden areas are the key urbanization indicators affecting extreme precipitation. (3) In the future scenarios, the duration and intensity characteristics of urban extreme precipitation will increase, and the growth rate will increase monotonically with the recurrence period.

**Keywords:** teleconnection factors; Henan Province; urban extreme precipitation; Granger causality test; urbanization indicators



**Citation:** Zhao, Y.; Tao, J.; Li, H.; Zuo, Q.; He, Y.; Du, W. Influence of Teleconnection Factors on Extreme Precipitation in Henan Province under Urbanization. *Water* **2023**, *15*, 3264. <https://doi.org/10.3390/w15183264>

Academic Editors: Qing Cao, Tiexi Chen and Shuci Liu

Received: 17 August 2023

Revised: 4 September 2023

Accepted: 7 September 2023

Published: 14 September 2023



**Copyright:** © 2023 by the authors. Licensee MDPI, Basel, Switzerland. This article is an open access article distributed under the terms and conditions of the Creative Commons Attribution (CC BY) license (<https://creativecommons.org/licenses/by/4.0/>).

## 1. Introduction

In recent years, global climate change has impacted atmospheric circulation worldwide, while human activities represented by urbanization have exacerbated underlying surface in urban areas prominently, especially aggravating the extremeness and harmfulness of urban precipitation events [1–3]. With the rapid development of urbanization, the corresponding research on extreme precipitation in urban regions has been gradually increasing, which mainly has the following characteristics. Firstly, the research objects are mainly typical agglomerations and highly urbanized areas, such as the Yangtze River Delta, Guangdong-Hong Kong-Macao Greater Bay Area, Beijing-Tianjin-Hebei region, and Tokyo, Seoul [4–6]. Zhang [7] noted that the increase in the intensity and frequency of extreme precipitation in cities due to rapid urbanization has been widely detected worldwide. Secondly, the research mainly focuses on analyzing the driving force of extreme precipitation in urban areas. Zhang et al. [8] explored urbanization effects on extreme precipitation using physical metrics including area, complexity, fragmentation, and dominance deduced from five periods of land use maps and found that magnitudes and frequencies are enhanced by them, especially in central urban region. Therefore, taking climate control and urbanization

as the driving force to analyze the impacts on urban extreme precipitation in typical cities or agglomerations is of practical significance.

It is crucial to separate the influence of one concerned driving force from the other when exploring the impact of different forces on urban precipitation. Relevant climate indexes can be adopted to characterize their independent function to isolate the influence of climate control on urban precipitation. Teleconnection refers to the significant correlation between meteorological anomalies in locations separated by a certain distance, typically spanning thousands of kilometers. Its main mechanism involves modifying local tropospheric temperatures, thereby altering large-scale pressure and wind fields or facilitating the cross-regional transfer of dust and other substances through wind movement. Silva et al. [9] validated the recognized teleconnection response of seasonal precipitation to sea surface temperature patterns (El Niño-Southern Oscillation) using the Granger causality test at different time scales. Yoo et al. [10] utilized teleconnection in the Northern Hemisphere to propose a composite statistical model for predicting the temperature within 6 weeks in East Asia during winter. Applying the teleconnection factor with inherent evolutionary mechanisms to characterize the contribution of climate control in quantitative attribution is an objective and credible approach. Commonly used approaches for identifying teleconnection include Pearson correlation coefficient, the Granger causality test, Copula analysis, and information entropy [11]. The separation of the impact of urbanization on urban precipitation can be classified into two main approaches: observation-based methods and model-based methods [5,12]. The observation-based methods primarily utilize statistical approaches for analysis [13,14], which have the advantage of removing the influence of climate system variability. On the other hand, model-based methods involve simulating and analyzing physical mechanisms using numerical weather models or theoretical physical models, which are mainly implemented in individual cases with limited universality. Song et al. [15] found that urbanization could induce the intensification of extreme precipitation, with a higher amount, intensity, and frequency of precipitation extremes and a larger magnitude of their trends in urban areas by comparison with those rural areas. Zhu et al. [16] analyzed the influence of urbanization on the spatial pattern and cause of hourly precipitation in Beijing through circular analysis and the Granger causality test and discovered that the urban areas with the highest population density exhibited longer duration, higher intensity, and larger magnitude. Paul et al. [17] analyzed the extreme precipitation in Mumbai, India, through WRF numerical simulations, and found that urbanization led to an enhanced magnitude of extreme precipitation. Given the aforementioned background, exploring the influence of teleconnection and urbanization on extreme precipitation in typical cities is of significant importance for understanding the inducing mechanisms of urban extreme precipitation and formulating corresponding prevention and control measures.

Henan Province is located in central China and serves as a vital transportation hub and a center for capital, logistics, and information flow. Henan Province is prone to experiencing heavy precipitation processes, and the occurrence of historical heavy rainstorm disasters was always attributed to typhoons, such as the “75.8” extremely heavy precipitation. The extreme precipitation event known as the “7.21” incident that occurred in July 2021 in Henan Province resulted in severe urban waterlogging disasters and significant social impacts [18]. Between 17 and 21 July 2021, Henan Province experienced a historically rare extreme rainfall event. The strongest period occurred from 08:00 on 19 July to 08:00 on 21 July, with the precipitation center predominantly concentrated in the central region of Henan Province, centered around Zhengzhou. The precipitation recorded at the Zhengzhou station on 20 July reached an astonishing 663.9 mm [19–21], and the three-day cumulative rainfall in most surrounding areas exceeded 400 mm, surpassing all historical records since the establishment of meteorological stations. Research based on reanalysis data and observational data has been conducted to analyze this extreme rainstorm event. The research findings indicate that stable atmospheric circulation patterns, abundant moisture and energy supply, pronounced terrain effects, as well as the continuous accumulation, merging,

and stagnation of convective systems in the precipitation area were the primary causes of this heavy rainfall event [22–24]. Deng et al. [25] pointed out that the binary typhoon Infa and Cempaka provided moist air parcels for “21.7” heavy rainfall in Henan province through numerical simulations. Wang et al. [26] determined the relationship between rainfall intensity and road-pipe overflow patterns based on “21.7” precipitation monitoring data. Zhao et al. [27] found that the upper-level synoptic-scale disturbance, which leads to the development of potential vorticity anomalies and its downward intrusion, played a critical role in the development of the “21.7” event. As a typical inland province in the central plains of China, the response of typical urban clusters in Henan Province to subtropical highs and typhoon reflects the teleconnection accurately. However, existing research has rarely been conducted from the perspective of teleconnection and focused on the typical inland urban clusters of Henan Province to reveal the impact of teleconnection on urban extreme precipitation under the urbanization.

This study selected nine typical cities in Henan Province to analyze the impact of teleconnection on urban extreme precipitation, based on precipitation data from 11 meteorological stations from 1951 to 2021 as well as 130 teleconnection factors. The dominant teleconnection factors, which influenced urban extreme precipitation in each city, were identified by the Granger causality test. Then, the precipitation characteristics were obtained by multiple linear regression and frequency analysis methods through comparing different driving force scenarios. Finally, the design values were calculated under various design frequencies based on the above, and the connection between 10 urbanization indicators and extreme precipitation was explored. This study aims to address the following specific questions: (1) What teleconnection factors dominate urban extreme precipitation, and do they exert common influence on disaster-affected cities? (2) What urbanization indicators are prominent in urban extreme precipitation? (3) What are the future variations?

The organization of this paper is as follows: Section 2 introduces the main methods used in this paper, including selection of statistical indicators, the Granger causality test, and the calculation of contribution; Section 3 briefly introduces the study area and used data; Section 4 is the results and discussions; Section 5 is the summary.

## 2. Methodology

This study is comprised of three steps taken to analyze the influence of teleconnection factors on extreme precipitation in Henan Province under urbanization (Figure 1):

Step1: Teleconnection identification. The nonstationarity of urban precipitation series was diagnosed by two nonparametric methods and the statistical characteristics were recognized. Then, the dominant teleconnection factors were selected through Granger causality test.

Step2: Interpreting attribution. The reconstructed precipitation series were simulated by virtue of relationship between teleconnection factors and precipitation, and the attributions are quantified under four different design frequencies. Then, the contribution was further interpreted by urbanization indicators.

Step3: Future prediction. The most optimal CMIP6 climate model for each city was selected and the future variation in extreme precipitation are predicted.

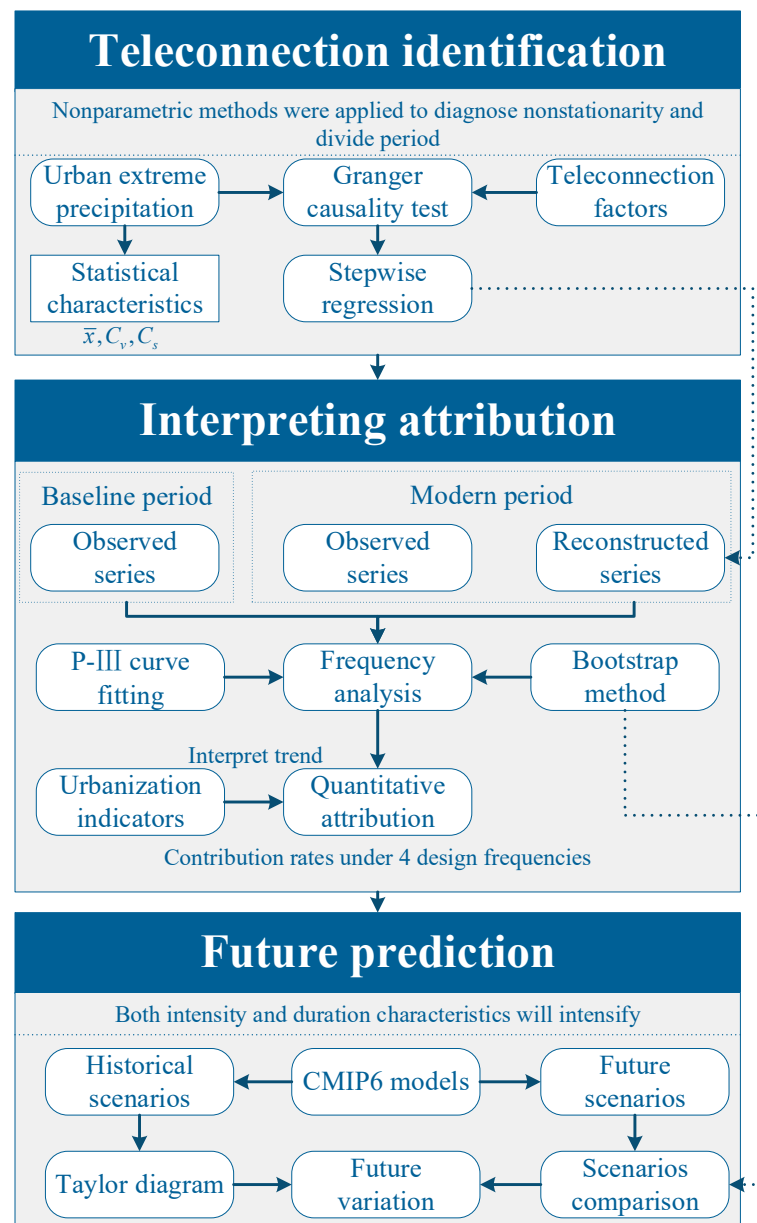


**Figure 1.** Flowchart for researching influence of teleconnection factors on urban extreme precipitation in Henan Province under urbanization.

2.1. Extreme Precipitation Connotation and Selection of Statistical Indicators

Extreme precipitation is one type of extreme event. Currently, there are five main methods internationally used to define extreme precipitation: the maximization method, the absolute threshold method, the standard deviation method, the percentile threshold method, and the membership degree method. Considering the “7.21” extreme precipitation event in Henan Province, where both the annual maximum one-day (AM1X) and annual maximum three-day (AM3X) precipitation exceeded historical records, this study selected these two indicators as the statistical metrics for extreme precipitation in Henan Province. The annual maximum method of sampling was used to derive data series consisting of the maximum precipitation at different windows across multiple stations over the years. Specifically, the AM1X and AM3X series at each station were obtained by arithmetic mean method and moving statistics method.

The statistical characteristics of the urban extreme precipitation series (mean,  $C_v$ ,  $C_s$ ) were obtained based on the three-parameter Pearson type III (P-III) distribution using

the curve-fitting method. The probability density function of P-III can be expressed by Equation (1):

$$f(x) = \frac{\beta^\alpha}{\Gamma(\alpha)} (x - a_0)^{\alpha-1} e^{-\beta(x-a_0)} \quad (1)$$

where  $\Gamma(\alpha)$  is the gamma function of  $\alpha$ ;  $\alpha$  is shape parameter;  $\beta$  is scale parameter;  $a_0$  is location parameter ( $\alpha > 0$  and  $\beta > 0$ ).

The bootstrap method [28] was used to overcome the uncertainty in the parameter estimation to obtain the design point values and interval estimation of the extreme precipitation at the four different design frequencies (0.01%, 0.1%, 1%, and 10%), which are key references for urban meteorological warning and engineering flood prevention.

## 2.2. Principle of Granger Causality Test

In order to characterize the role of climate control, previous studies usually selected fundamental hydrological elements (such as evaporation, temperature, etc.) as climate indicators. However, the basic hydrological elements are also influenced by human activities, especially in urban areas. Therefore, it is inaccurate to rely solely on basic hydrological elements to represent the impact of climate control on extreme precipitation in urban areas. Therefore, this study utilizes teleconnection factors, with internal evolving mechanisms which are less influenced by human activities, to represent the influence of climate control. The relationship between teleconnection factors and extreme precipitation are identified using the Granger causality test.

The Granger causality test method is used to detect the causal relationship between two time series,  $X$  and  $Y$  ( $i = 1, \dots, m$ ) [29]. The model is shown in Equations (2) and (3): if  $X$  causes changes in  $Y$ , the overall  $\alpha$  value is not equal to 0, and the overall  $\lambda$  value is equal to 0; if  $Y$  causes changes in  $X$ , the overall  $\alpha$  value is equal to 0, and the overall  $\lambda$  value is not equal to 0; if  $X$  and  $Y$  are mutually causal, the overall value of the  $\alpha$  and  $\lambda$  are not equal to 0; if  $X$  and  $Y$  are independent of each other, the overall value of the  $\alpha$  and  $\lambda$  are equal to 0.

$$Y_t = \sum_{i=1}^m \alpha_i X_{t-i} + \sum_{i=1}^m \beta_i Y_{t-i} + \mu_{1t} \quad (2)$$

$$X_t = \sum_{i=1}^m \lambda_i Y_{t-i} + \sum_{i=1}^m \delta_i X_{t-i} + \mu_{2t} \quad (3)$$

where  $\alpha$ ,  $\beta$ ,  $\lambda$ , and  $\delta$  are model coefficients;  $\mu_{1t}$  and  $\mu_{2t}$  are model white noise, assuming they are uncorrelated. In this study, the series  $X$  represents each teleconnection factor, and the series  $Y$  represents urban extreme precipitation.

## 2.3. Contribution of Teleconnection Factors and Urbanization to Urban Extreme Precipitation

The impact of teleconnection factors and urbanization on extreme precipitation at different frequencies can be quantified by Equations (4) and (5) realized by the form of contribution rates, where the contribution of urbanization can be reflected by the difference between reconstructed values and observed values.

$$r_c = \frac{|pre_c|}{|pre_c| + |pre_h|} \times 100\% \quad (4)$$

$$r_h = \frac{|pre_h|}{|pre_c| + |pre_h|} \times 100\% \quad (5)$$

where  $pre_c$  denotes the design value obtained from the frequency analysis;  $pre_h$  denotes the difference between the observed value and the design value during the modern period;  $r_c$  denotes the contribution of teleconnection factors to extreme precipitation; and  $r_h$  denotes the contribution of urbanization to extreme precipitation.

### 3. Case Study

#### 3.1. Study Area

The study areas selected in are shown in Figure 2. According to the administrative divisions, Zhengzhou, Anyang, Xinxiang, Kaifeng, Luoyang, Pingdingshan, Xuchang, Zhoukou, and Nanyang City in Henan Province are included, all of which are within the impact range of “21.7” extreme rainstorm in Henan Province [30,31].

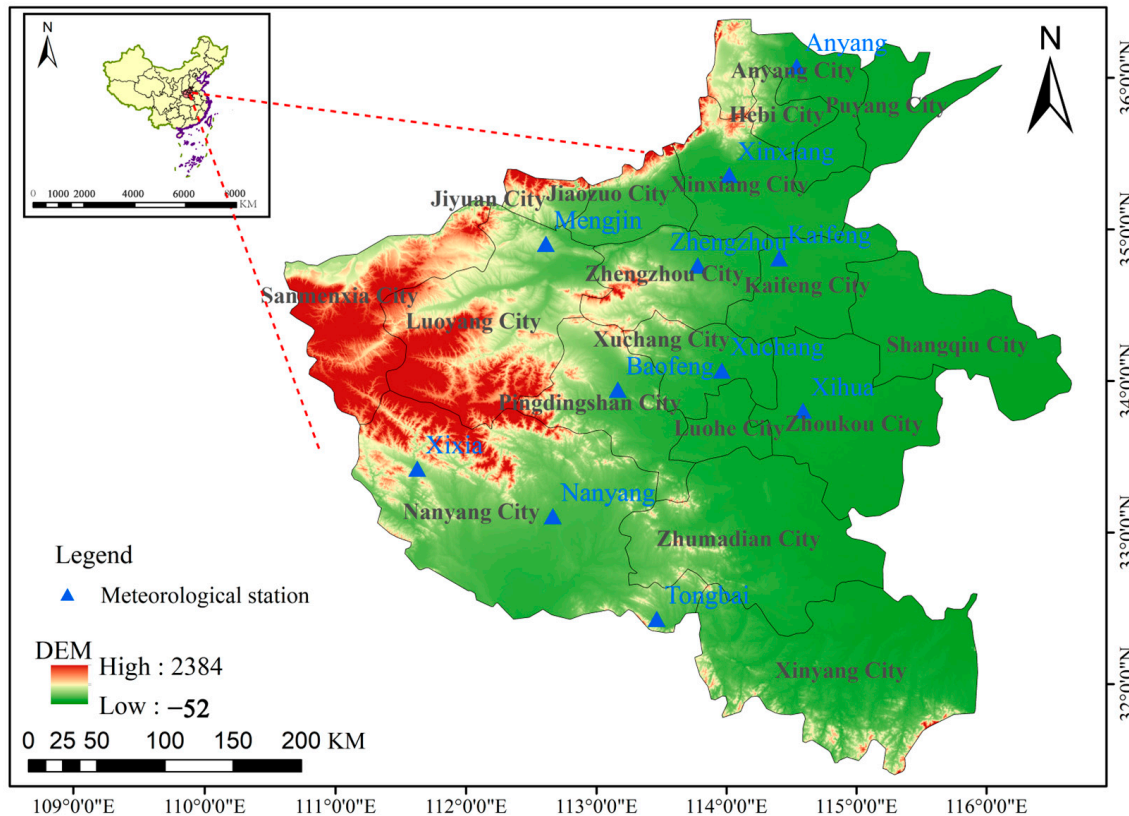


**Figure 2.** Location of the study area and layout of stations.

Henan province is a typical inland province, it is located in the western transitional zone of the Yellow-Huai River plain. The climate is shifted from the warm semi-humid temperate in the north to the North Subtropical climate in the south, and terrain is transformed from hilly and mountainous in the west to plain in the east. Heavy rainstorm in Henan Province exhibits distinct seasonal and regional characteristics, with an average annual precipitation range from 407.7 to 1295.8 mm, which is concentrated from June to August. In terms of spatial distribution, the days and the amount of heavy rainstorms generally decrease from east to west and from south to north. Meanwhile, Henan Province is the most populous province in China and has undergone rapid urban expansion. The permanent resident population has grown from 13.49 million in 1950 to 98.83 million in 2021, and the urbanization rate has increased from 6.8% in 1950 to 56.45% in 2021.

#### 3.2. Data

The precipitation data of 11 stations covering 9 cities and teleconnection factors including 130 items were sourced from National Climate Center (NCC). The climate models of CMIP6 were retrieved at the Inter-Sectoral Impact Model Intercomparison Project (ISIMIP). This contains daily historical data (1951–2014) and simulation data for the future (2015–2100), and there are four future period scenarios (SSP1-2.6, SSP2-4.5, SSP3-7.0, SSP5-8.5) according to the differences in shared socio-economic paths, which represent the multifarious participation level of human activities. Statistical downscaling and bias

correction have been implemented in each CMIP6 model, and all of the CMIP6 models are downscaled from their original resolution in Table 1 to  $0.5^\circ \times 0.5^\circ$ .

The data of 10 urbanization indicators were sourced from China Economic and Social Big Data Research Platform and Henan Statistical Yearbook [32]. Due to disclosure restrictions, only 21 years of data from 2001 to 2021 could be downloaded.

The detailed properties of multiproxy data are summarized in Table 1.

**Table 1.** Details of data properties.

Data Type	Detail	Source	Scale	Span	
Precipitation	Zhengzhou (Zhengzhou City), Xinxiang (Xinxiang City), Mengjin (Luoyang City), Nanyang (Nanyang city), Tongbai (Nanyang City), Xixia (Nanyang City), Baofeng (Pingdingshan City), Anyang (Anyang City), Xuchang (Xuchang City), Kaifeng (Kaifeng City), Xihua (Zhoukou City)	NCC	Daily	1951–2021	
Teleconnection factors	88 atmospheric circulation indexes, 26 Sea Surface Temperature (SST) indexes, 16 other indexes	NCC	Monthly	1951–2021	
GCMs	IPSL-CM6A-LR	Institute Pierre-Simon Laplace (IPSL), Europe	$2.5^\circ \times 1.26^\circ$	1951–2100	
	MRI-ESM2-0	Meteorological Research Institute (MRI), Japan	$1.125^\circ \times 1.125^\circ$	1951–2100	
	CNRM-ESM2-1	CNRM-CERFACS, France	$1.4^\circ \times 1.4^\circ$	1951–2100	
	CanESM5	Canadian Centre for Climate Modelling and Analysis (CCCma), Canada	$2.8^\circ \times 2.8^\circ$	1951–2100	
Urbanization indicators	Urbanization rate, population density, per capita GDP, built-up district area, built-up areas density of water pipes, density of sewers in built district, green coverage rate of built-up district, length of road, road area, botanical garden areas	MIROC6	MIROC, Japan	$1.4^\circ \times 1.4^\circ$	1951–2100
			Statistical yearbook of Henan province	Yearly	2001–2021
		China economic and social big data research platform	Yearly	2001–2021	

## 4. Results and Discussion

### 4.1. Temporal and Spatial Variations of Urban Extreme Precipitation under Urbanization

The Mann-Kendall [33,34] and Pettitt test [35] were applied to examine the stationarity of precipitation series. The common results in two kinds of tests were regarded as mutation points, while mutation points were selected according to the series length and the actual situations when the different results were obtained. The mutation points for the 11 stations are listed as Table 2. According to the temporal variations in urban extreme precipitation series, the study area could be roughly divided into four categories (Figure 3), that is, area whose mutation points occurred around 2001 including Mengjin, Zhengzhou, Xinxiang, and Anyang; area whose mutation points occurred around 1983, including Baofeng, Xixia, and Kaifeng; area whose mutation points occurred around 1991, including Xuchang and Xihua; and area whose mutation points occurred around 2012, including Nanyang and Tongbai. In particular, the temporal variation in urban extreme precipitation was represented by nonstationarity in time series, which reflected the time-dependent node when urbanization played a significant role in urban extreme precipitation. The spatial variation was represented by the common category for mutation point in different cities, which reflected the regional scope of urbanization impact on urban extreme precipitation. Figure 3 shows that the information of the distribution of cities in the same category is continuous, which indicates that the region impact of urbanization exists.

Figure 3 shows the trends of urban extreme precipitation before and after the mutation point. Urban extreme precipitation increases or decreases gently before the mutation point; however, (1) in the areas where the mutation points are around 2001, there are sharp growths after the mutation point (the most significant in Zhengzhou); (2) in the areas where the mutation points are around 1983, the trends show a gentle upward trend after the mutation point; (3) in the areas where the mutation points are around 1991, there are downward trends after the mutation point; and (4) in the areas where the mutation points are around 2012, the trends increase sharply in Tongbai and decrease in Nanyang.

Henan province straddles the south–north climate transition zone and is deeply affected by monsoon climate. The southern region, located near the Qinling Mountains and Huaihe River, belongs to the north subtropical monsoon climate region, with abundant precipitation and long rainy seasons. The incidence of heavy rainfall is low in the northwestern region because the continental climate is strong, and it is relatively difficult for the monsoon to penetrate. Influenced by the seasonal variation in atmospheric circulation and the difference in latitudes and terrain between north and south, the precipitation contour of Henan Province shows an east–west trend, while the plain area shows a northeast-to-southwest trend.

The formation of extreme precipitation requires three basic conditions: water vapor condition, unstable structure, and uplift condition. The extreme precipitation in Henan province mainly occurs in June, July, and August. There are three main types of weather conditions: marginal high subtropical type, low trough type, and northwest airflow type; the first two weather conditions appeared more frequent and concentrated in July and August, the last weather condition appeared less frequent and concentrated in June. In detail, the main characteristics of the marginal subtropical high type include that the subtropical high is strong, the lower level is warm humid moisture, and the water vapor transport conditions are sufficient. The main characteristics of the low trough type are that the positive vorticity advection in front of the 500 hPa low trough provides better upper-level dynamic conditions for the development of strong convection, while the development of the low-level Southerly jet provides more favorable temperature and humidity stratification conditions.

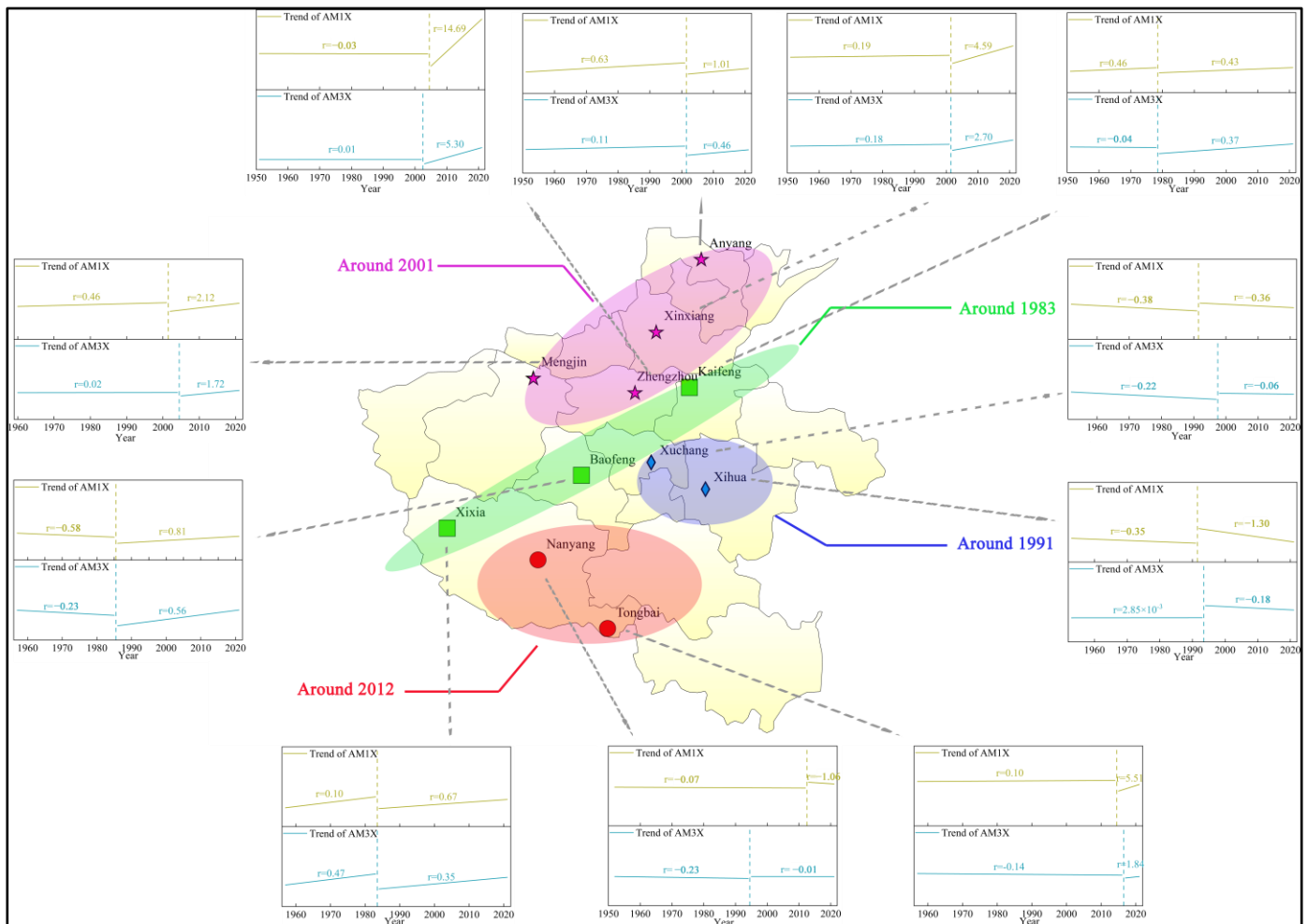


Figure 3. The trend and spatial pattern of nonstationarity in extreme precipitation.

**Table 2.** The diagnosed results of nonstationary precipitation series.

Station	Mutation Point of AM1X Series (Year)	Mutation Point of AM3X Series (Year)
Zhengzhou	2004	2002
Xinxiang	2001	2001
Mengjin	2001	2004
Nanyang	2012	1994
Tongbai	2014	2016
Xixia	1983	1983
Baofeng	1985	1985
Anyang	2001	2001
Xuchang	1991	1997
Kaifeng	1978	1978
Xihua	1991	1993

#### 4.2. The Dominant Teleconnection Factors of Urban Extreme Precipitation

It is assumed that the stationarity of the urban extreme precipitation series was broken by urbanization when this force accumulated to be largely enough, and this time node was defined as the mutation point. Based on the above assumptions, the period before the mutation point is defined as the “baseline period” when urbanization is weak and negligible, and only the teleconnection dominates precipitation. The period after the mutation point is defined as the “modern period” when urbanization begins to have a significant impact and is also taken into account. In the baseline period, the Granger causality test was used to identify the dominant teleconnection factors affecting urban extreme precipitation with a set time lag of 0–12 months. The results show that the AM1X in Zhengzhou, Xinxiang, Mengjin, Nanyang, and Anyang are more sensitive to teleconnection factors than the AM3X, that is there are more teleconnection factors owning notable Granger causality with AM1X than AM3X; meanwhile, the AM3X in Tongbai, Xixia, Baofeng, Xuchang, Kaifeng, and Xihua are more sensitive to the teleconnection factors than the AM1X. Furthermore, the response pattern to teleconnection over the above cities corresponds to the spatial pattern in Figure 3. This indicates that teleconnection also exists in the region impact aside from urbanization as mentioned in Section 4.1, which reflects the fact that teleconnection always influences the same urban extreme precipitation indicators (AM1X or AM3X) within the same category in Figure 3.

In order to eliminate collinearity among the factors, stepwise regression was used to optimize the identified factors and find out the most explanatory independent variables. Then, multiple linear regression models were constructed by the most germane teleconnection factors without considering urbanization (Table 3). We can see from Table 3 that atmospheric circulation indexes are most considerable in teleconnection, and the more atmospheric the circulation indexes are, the better model interpretation ability is. SST indexes are more notable than other indexes generally. In addition, the results show that the influence of teleconnection factors on urban extreme precipitation appears to be on regional common characteristics, which means that the same factors affect multiple cities in the same category region in Figure 3. For instance, the West Pacific 850 mb Trade Wind Index (zonal wind average standardized value in 850 hPa zonal wind field, 5° N–5° S, 135° E–180° W), East Pacific 850 mb Trade Wind Index (zonal wind average standardized value in 850 hPa zonal wind field, 5° N–5° S, 135° W–120° W), Atlantic Multi-decadal Oscillation Index (regional average of sea surface temperature anomaly in the 0° N–70° N and 80° W–0° W region), Antarctic Oscillation Index (the normalized sequence of the time coefficients of the first mode obtained from the empirical orthogonal function analysis (EOF) of the anomaly field at a height of 700 hPa in the region of 20°–90° S and 0°–360°), Western Pacific Subtropical High Intensity Index (the cumulative values of the difference between the geopotential height and 5870 geopotential meters multiplying the cell area, within the range >5880 geopotential meters in 500 hPa field, 10° N–60° N, 110° E–180° E), Indian Ocean Basin-Wide Index (regional average value of sea surface temperature anomaly in the

20° S–20° N and 40°–110° E region), Northern Hemisphere Polar Vortex Central Latitude Index (the latitude position of the center of a low vortex with the lowest geopotential height in the high latitude region of 550 hPa altitude field of northern hemisphere), and another 22 teleconnection factors exert significant influence on the urban extreme precipitation of two or more cities in the Xixia-Baofeng-Kaifeng region. Three teleconnection factors, namely Atlantic-European Polar Vortex Area Index (the sector area enclosed north of the characteristic contours of the polar vortex southern boundary, in the 500 hPa height field of the northern hemisphere, 30° W–60° E), West Pacific 850 mb Trade Wind Index and Tropical Northern Atlantic SST Index (regional average value of sea surface temperature anomaly in the 5.5° N–23.5° N, 57.5° W–15° W region) exert the simultaneous influence on urban extreme precipitation of Zhengzhou-Xinxiang-Mengjin-Anyang region. Three teleconnection factors, namely the West Wind Drift Current SST Index (regional average value of sea surface temperature anomaly in the 35° N–45° N, 160° E–160° W region), NINO B SSTA Index (regional average value of sea surface temperature anomaly in the 0°–10° N, 50° E–90° E region), and South Indian Ocean Dipole Index (the difference between the regional average value of sea surface temperature anomaly in the 45° S–30° S and 45° E–75° E regions and the 25° S–15° S and 80° E–100° E regions) exert influence on urban extreme precipitation in the Xuchang-Xihua region. The Asian Meridional Circulation Index (the average meridional index of three regions which is divided at 30 longitude intervals in the 500 hPa altitude field, 45° N–65° N and 60° E–150° E) affects the urban extreme precipitation in Nanyang and Tongbai. The urban extreme precipitation series, which is assumed to be only affected by teleconnection, of every station in the modern period was reconstructed based on the regression models.

**Table 3.** Functional relationship between extreme precipitation and teleconnection factors in typical cities.

Station	Series	Atmospheric Circulation Indexes	SST Indexes	Other Indexes	R <sup>2</sup>	p
Zhengzhou	AM1X	3	0	0	0.281	8.31 × 10 <sup>-4</sup>
	AM3X	1	1	2	0.468	4.33 × 10 <sup>-6</sup>
Xinxiang	AM1X	4	0	1	0.548	9.32 × 10 <sup>-7</sup>
	AM3X	4	1	1	0.528	5.70 × 10 <sup>-6</sup>
Mengjin	AM1X	1	0	1	0.336	4.12 × 10 <sup>-4</sup>
	AM3X	1	1	1	0.395	1.44 × 10 <sup>-4</sup>
Nanyang	AM1X	3	0	1	0.485	6.75 × 10 <sup>-7</sup>
	AM3X	4	1	0	0.520	4.63 × 10 <sup>-5</sup>
Tongbai	AM1X	2	1	0	0.280	5.451 × 10 <sup>-4</sup>
	AM3X	6	1	0	0.535	8.73 × 10 <sup>-7</sup>
Xixia	AM1X	16	7	1	1.000	1.16 × 10 <sup>-7</sup>
	AM3X	11	2	0	0.995	1.11 × 10 <sup>-11</sup>
Baofeng	AM1X	22	3	1	1.000	4.14 × 10 <sup>-7</sup>
	AM3X	18	5	3	1.000	1.75 × 10 <sup>-8</sup>
Anyang	AM1X	6	2	0	0.658	1.62 × 10 <sup>-7</sup>
	AM3X	1	0	0	0.084	4.07 × 10 <sup>-2</sup>
Xuchang	AM1X	6	1	0	0.688	2.25 × 10 <sup>-6</sup>
	AM3X	7	8	0	0.903	9.24 × 10 <sup>-11</sup>
Kaifeng	AM1X	21	3	1	1.000	6.47 × 10 <sup>-7</sup>
	AM3X	1	0	0	0.171	2.89 × 10 <sup>-2</sup>
Xihua	AM1X	0	1	1	0.286	2.32 × 10 <sup>-3</sup>
	AM3X	3	3	1	0.745	6.34 × 10 <sup>-8</sup>

According to the previous literature, the main source of water vapor flux for summer precipitation in North China is the western Pacific Ocean, the South China Sea, and the mid-high latitude westerlies, while the water vapor from the Bay of Bengal also has a certain strengthening effect on heavy rainfall. Furthermore, at 500 hPa altitude field, the southwest flow is dominant in the west of the subtropical high when the center of the

subtropical high is in the west to the north, which can carry a lot of water vapor to the North China.

#### 4.3. The Influence of Teleconnection on Urban Extreme Precipitation under Urbanization

In order to quantify the effects of teleconnection and urbanization on urban extreme precipitation in different design frequencies, frequency analysis was carried out on the observed values of AM1X and AM3X series in the baseline period, modern period, and the whole period, as well as the reconstructed values in the modern period. In detail, there are two steps in frequency analysis; Pearson-III distribution was adopted for curve fitting and the bootstrap method was applied to reduce uncertainty in the representation of samples. The design values of urban extreme precipitation under four frequencies of 10%, 1%, 0.1%, and 0.01% were deduced. Specifically, the statistical characteristic parameters of the urban extreme precipitation series in every city are listed in Table 4, and have been compared with the Rainstorm Atlas and Parameter Description of Henan Province to confirm the rationality.

**Table 4.** Statistical characteristics of extreme precipitation in typical cities.

	AM1X			AM3X		
	$C_v$	$C_s$	Mean (mm)	$C_v$	$C_s$	Mean (mm)
Zhengzhou	1.15	7.38	92.86	1.11	7.28	40.95
Xinxiang	0.65	3.23	87.15	0.67	2.35	39.65
Mengjin	0.39	1.05	69.24	0.39	1.77	32.59
Nanyang	0.39	1.13	94.55	0.47	2.53	43.10
Tongbai	0.47	1.61	121.17	0.49	1.79	56.27
Xixia	0.41	1.76	84.33	0.41	1.84	38.07
Baofeng	0.50	2.06	90.82	0.46	1.39	40.51
Anyang	0.52	1.74	85.28	0.51	1.63	39.05
Xuchang	0.40	0.99	83.52	0.41	1.63	38.31
Kaifeng	0.50	1.55	89.57	0.50	1.77	39.77
Xihua	0.39	1.27	91.86	0.44	1.08	41.79

The point and interval estimation of the design values for the urban extreme precipitation series in three kinds of period (baseline, modern, and future) under four design frequencies, deduced by bootstrap method and P-III distribution, are exhibited in Figure 4. It should be noted that the order of the stations in every period is the same as that in Table 3, and that SSP2-4.5 scenario does not exist in some CMIP6 climate models in the future period, with the future predicted value being represented by multi-model ensemble mean, and only the design values of the observed period being marked because of the overshoot reconstructed series of Tongbai County.

Figure 4 shows the information of difference between urban extreme precipitation in the baseline and modern period, with the influence of teleconnection reflected in the observed series and the influence of urbanization is reflected in reconstructed series. In terms of the influence of teleconnection, most design urban extreme precipitation in different frequencies has no significant change, except for Xinxiang compared with the baseline period. In terms of the influence of urbanization, it was established that urban extreme precipitation has been aggravated in different frequencies by urbanization from the mutation point onward, which is reflected in the considerable design value of reconstructed series in modern period.

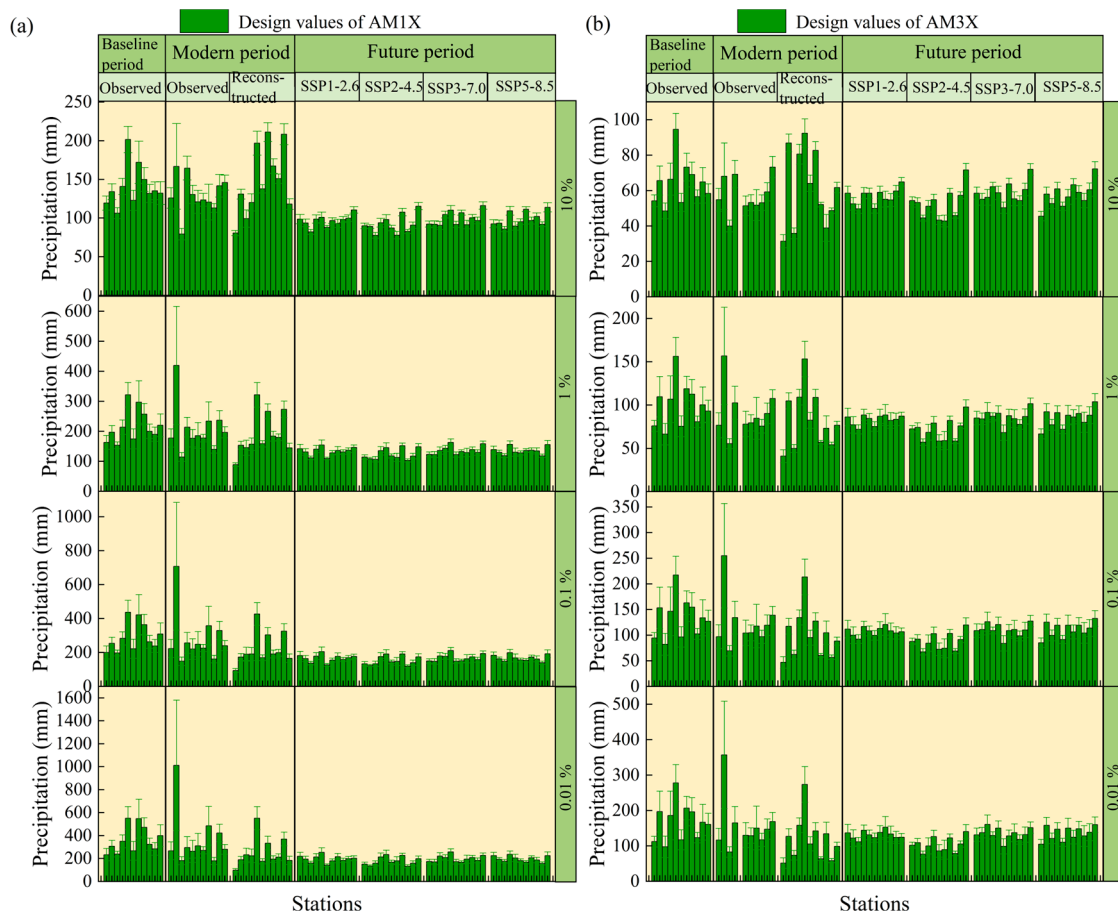


Figure 4. Design precipitations and interval estimation with design frequency of 10%, 1%, 0.1%, 0.01%: (a) results of AM1X; (b) results of AM3X.

The contribution of teleconnection and urbanization to urban extreme precipitation under four design frequencies is shown in Figure 5. It can be seen that the main driving force of extreme precipitation in most cities is teleconnection factors, which account for 50.3–99.8%. In terms of spatial distribution, from the contribution rates of urbanization emerges a radial distribution with an overall decrease in central and southern regions as well as an overall increase in other marginal regions. The major results are as follows:

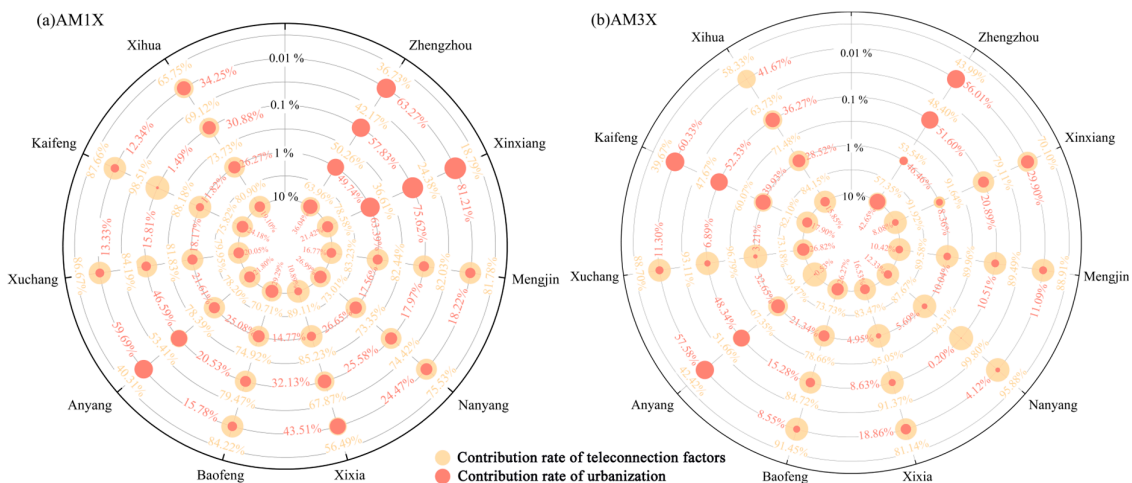
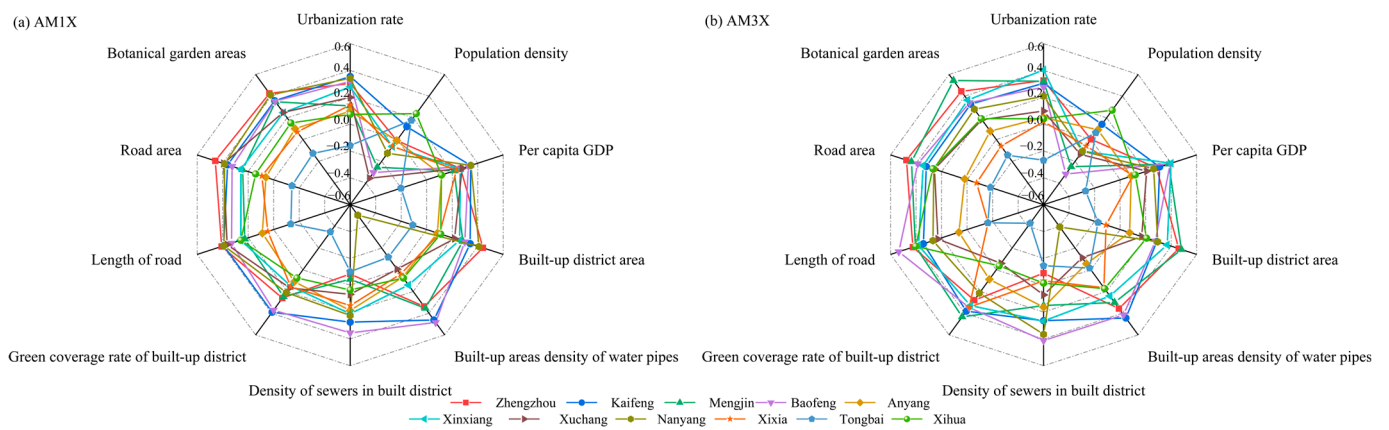


Figure 5. The contribution rates of teleconnection factors and urbanization to urban extreme precipitation under different frequency.

a. On the whole, the influence of teleconnection factors on AM3X is higher than that on AM1X, especially for the precipitation of the following stations with specific design frequency, and the increments of the contribution rates were calculated: (1) the precipitation of Xinxiang, Mengjin, Nanyang, and Baofeng at four frequencies, had a respective increase of +13.3–+55.0%, +6.4–+7.6%, +14.7–+25.4%, +3.0–+7.2%; (2) the precipitation of Zhengzhou, XiXia, and Xuchang under the frequency of 1%, 0.1%, and 0.01%, had a respective increment of +3.2–+7.3%, +9.8–+24.6%, and +2.0–+15%; (3) the precipitation of Kaifeng and Xihua under the frequency of 10%, had an increment of +6.3% and +3.3%; (4) the precipitation of Anyang under the frequency of 10% and 0.01%, had a respective increment of +21.3% and +2.1%. Conversely, the influence of teleconnection factors on AM1X is higher than that on AM3X for the remaining stations and design frequencies.

b. The quantitative contribution also presents trend variations in the recurrence period of design precipitation. It can be seen from Figure 5 that, with the increase in the recurrence period, (1) the influence of teleconnection on AM1X in Zhengzhou, Xinxiang, Xihua, and Xixia, as well as the AM3X in Zhengzhou, Xinxiang, Xihua, Anyang, and Kaifeng, decreases monotonously, while the influence of urbanization increases monotonically. (2) The influence of teleconnection and urbanization on AM1X in Mengjin and Nanyang and AM3X in Mengjin is almost stable, with a change in contribution rate of less than 3%. (3) The influence of teleconnection on the AM1X in Baofeng (from 70.7% to 84.2%) and Xuchang (from 80.0% to 86.7%), and the AM3X in Baofeng (from 73.7% to 91.4%), increases monotonically, but the influence of urbanization decreases monotonically. Considering that different areas have different levels of urbanization, that is to say, the influence degree of urbanization on extreme precipitation is individual. Thus, these trend variations in quantitative contribution are attributed to inconsistent the urbanization level, which is concreted by urbanization indicators.

c. The sensitive urbanization indicators of every typical city are relatively consistent. The correlation coefficient between urbanization indicators and urban extreme precipitation is calculated individually for every city, and the results are shown in Figure 6. In a clockwise manner, in Figure 6, the most impressionable areas for each urbanization indicator to urban extreme precipitation are: (1) Kaifeng, Xihua, Nanyang, Zhengzhou, Baofeng, Baofeng, Kaifeng, Zhengzhou, Zhengzhou, and Zhengzhou, for AM1X, respectively; (2) Xinxiang, Xihua, Xinxiang, Mengjin, Kaifeng, Baofeng, Mengjin, Baofeng, Zhengzhou, and Mengjin, for AM3X, respectively. In particular, the AM3X in Mengjin is remarkably relevant to botanical garden areas ( $r = 0.54$ ,  $p = 1.09 \times 10^{-2}$ ) and built-up district areas ( $r = 0.48$ ,  $p = 2.73 \times 10^{-2}$ ) compared with AM1X. AM3X in Baofeng has the same situation with length of road ( $r = 0.54$ ,  $p = 1.24 \times 10^{-2}$ ) compared with AM1X, which should be paid high attention in local rainstorm and flood management. The four main communal indicators affecting urban extreme precipitation are road area, built-up district area, botanical garden areas, and length of road, which directly reflect the state of urban impervious underlying surface and have significant impact on urban hydrological cycle. Among them, the extreme precipitation in Zhengzhou, Kaifeng, Mengjin, Baofeng, Xinxiang, and Nanyang presents strong relation to the urbanization indicators, showing a high correlation level with most urbanization indicators. The correlation between extreme precipitation and the urbanization indicators is relatively weak in Anyang, Xuchang, Xihua, Xixia, and Tongbai. At the same time, the trend changes in quantitative attribution are also highly correlated with the level of urbanization. In areas with a high urbanization level, the influence of urbanization indicators on extreme precipitation increases significantly with the recurrence period and decreases significantly with the reverse. Taking Zhengzhou City (Zhengzhou Station) and Pingdingshan City (Baofeng Station) as examples, the impact of urbanization on extreme precipitation in Zhengzhou City also increases with the recurrence period. On the contrary, the impact of urbanization on extreme precipitation in Pingdingshan City decreases with the recurrence period (Figure 7).



**Figure 6.** Analysis of importance of different urbanization indicators to extreme precipitation in typical cities of Henan Province.

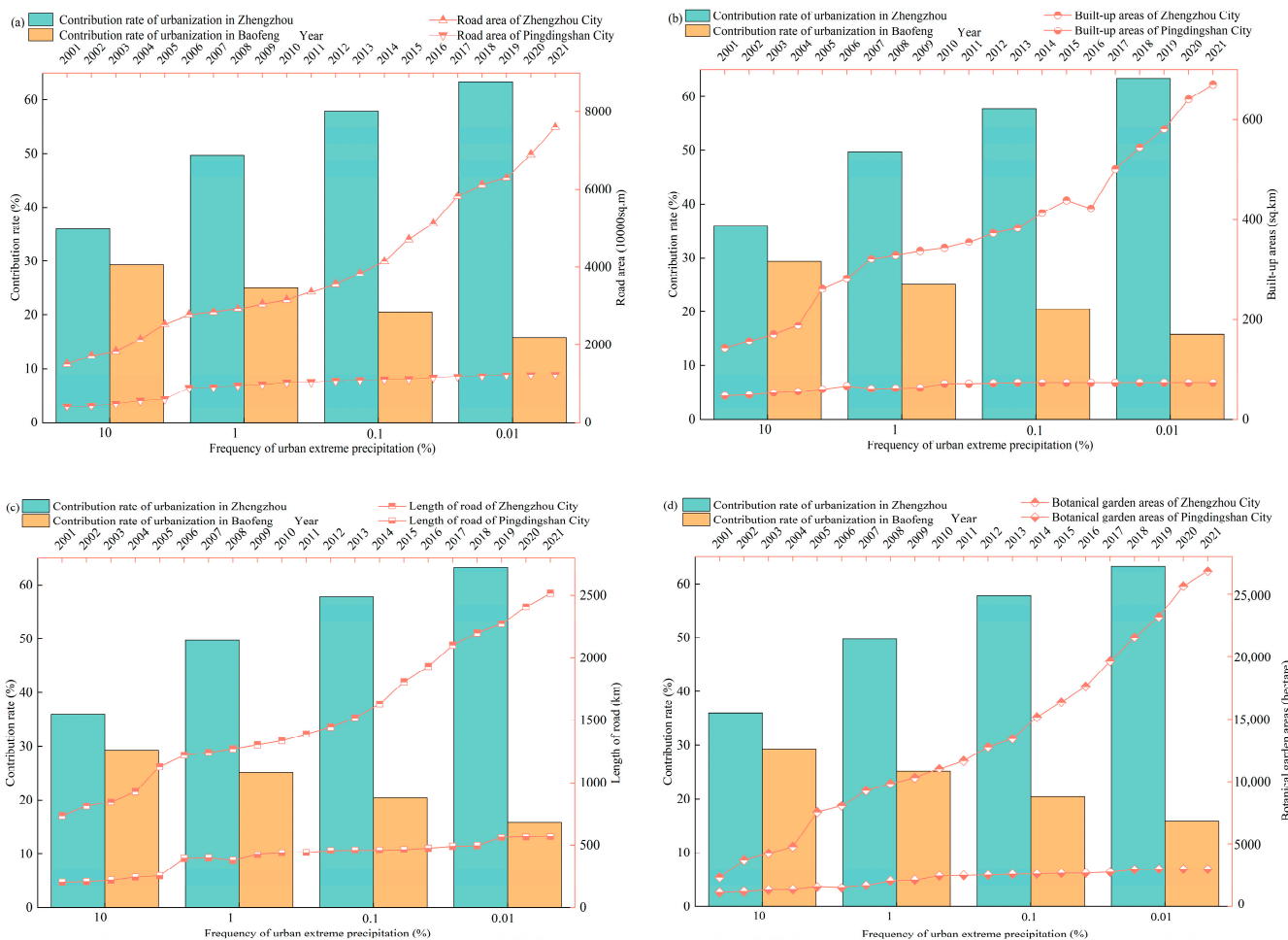


**Figure 7.** Relationship between urbanization indicators and contribution rates of urbanization: (a) road area; (b) built-up areas; (c) length of road; (d) botanical garden areas.

d. Therefore, for the above typical cities in Henan Province, teleconnection factors should be considered in the urban precipitation forecast to improve precision on the basis of considering the urban climate and geographical situations. Meanwhile, engineering measures should be strengthened according to local conditions and the corresponding sensitive indicators of each city, on the basis of improving the common shortcomings of prevention and control for urban extreme precipitation disaster. Moreover, urbanization

indicators, including area of built-up districts, length of roads, area of roads, and botanical garden areas, are highly relevant to urban extreme precipitation and all of which need prudent decision making in urban planning and construction.

4.4. Prediction of Future Extreme Precipitation

Five climate models of CMIP6 were assessed as alternatives, and the climate model with the best analog ability was selected for every station by virtue of the Taylor diagram [36] in Figure 8, which is listed in Table 5.

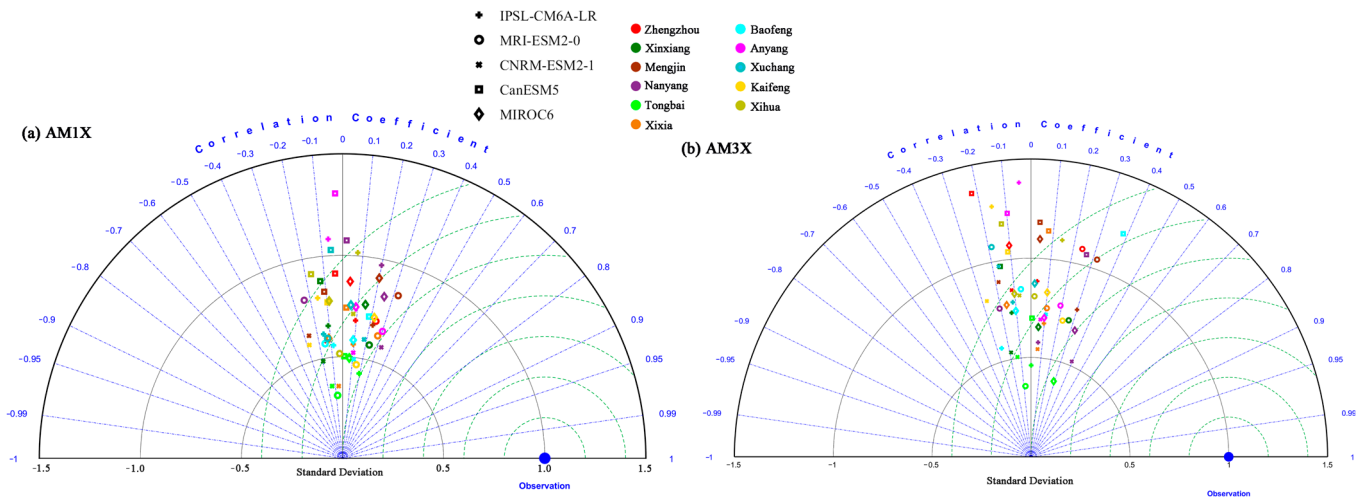


Figure 8. Evaluation of CMIP6 climate models by Taylor diagrams.

Table 5. The best fitted CMIP6 climate model of cities.

Station	AM1X	AM3X
Zhengzhou	MRI-ESM2-0	MRI-ESM2-0
Xinxiang	MRI-ESM2-0	MRI-ESM2-0
Mengjin	MRI-ESM2-0	MRI-ESM2-0
Nanyang	CNRM-ESM2-1	CNRM-ESM2-1
Tongbai	IPSL-CM6A-LR	MIROC6
Xixia	MRI-ESM2-0	CNRM-ESM2-1
Baofeng	MRI-ESM2-0	CNRM-ESM2-1
Anyang	MRI-ESM2-0	MRI-ESM2-0
Xuchang	CNRM-ESM2-1	MIROC6

After identifying the best CMIP6 climate model for every city, the extreme precipitation series regenerated from four future scenarios (SSP1-2.6, SSP2-4.5, SSP3-7.0, SSP5-8.5) were compared with the observed series to predict the future variation. Likewise, the AM1X and AM3X series were obtained by the arithmetic mean method and moving statistics method sampling from four future scenarios. Then, the bootstrap method and P-III curve fitting were used to obtain the design values of urban extreme precipitation with 10%, 1%, 0.1%, and 0.01% frequencies of every city under different future scenarios (2015–2100). As shown on the right-hand side of Figure 4, the difference between future and observed urban extreme precipitation series of each city in every period can be obtained. Generally, the enhancement of urban extreme precipitation within different frequencies in each area will be relatively stable, and the maximum precipitation will appear in Xihua, except for AM1X in 0.1% and 0.01% of Nanyang.

Figure 9 presents the specific change rate of urban extreme precipitation under different frequencies by comparing the design values in future and observed conditions. In detail, the design value of urban extreme precipitation in the future under different frequencies was obtained by arithmetic mean method from all future scenarios, and the

observed condition under different frequencies was obtained from the whole period. As for most areas in the future, the variation rates of the AM1X and AM3X show a monotonically increasing trend with the increase in the recurrence period, that is, the variation degree of the extreme precipitation with the increase in the recurrence period. However, the variation rates of the AM3X in Mengjin and Xuchang decrease monotonically with the increase in the recurrence period. It is supposed, as a premise, that the intensity characteristics are reflected by AM1X and the duration characteristics are reflected by AM3X. Compared with the observed period, the duration and intensity of future extreme precipitation will increase in most regions under different frequencies, except for the intensity of Zhengzhou and the duration of Mengjin. Under different frequencies, the most significant increases in intensity were found in Xinxiang (37.20–62.55%), Tongbai (49.28–55.72%), Anyang (32.05–55.14%), and Kaifeng (32.79–51.79%), while the most significant increases in duration were found in Xinxiang (18.58–42.25%) and Tongbai (30.94–41.72%). With the increase in the recurrence period, the change rate of intensity is the fastest in Xihua (2.14 times), and the change rate of duration is the fastest in Zhengzhou (39.40 times).

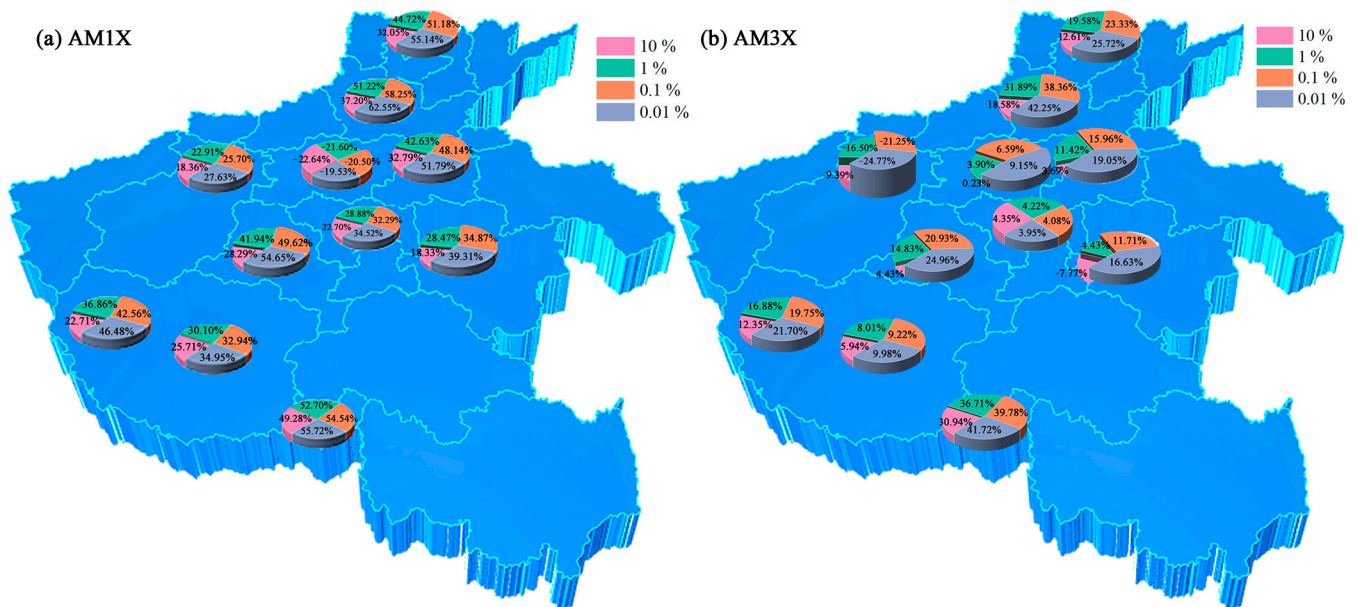


Figure 9. The future change in urban extreme precipitation under different frequency.

Based on the above analysis, extreme precipitation in the typical cities of Henan Province will intensify in the future, so the drainage standards of urban drainage facilities should be further improved, and the urban development level and the capacity of urban rainstorm and flood prevention should be taken into account integrally.

### 5. Conclusions

This study proposes a new theoretical frame to interpret the attribution of urban extreme precipitation from the perspective of teleconnection under the condition of urbanization. First, urban extreme precipitation series were diagnosed, and statistical characteristics were recognized. Then, dominant teleconnection factors were identified using Granger causality tests. Subsequently, design precipitation under four design frequencies was derived by the bootstrap method and P-III curve fitting, and quantitative attribution of urban extreme precipitation was realized by comparing the reconstructed series by applying teleconnection factors and the observation series. Meanwhile, essential urbanization indicators were recognized, which were purposed to interpret the trend of quantitative attribution. Finally, the future variations in urban extreme precipitation were obtained from the CMIP6. The conclusions were drawn as follows:

(1) There are obvious regional commonalities in the teleconnection factors controlling urban extreme precipitation, such as the West Pacific 850 mb Trade Wind Index and the Western Pacific Subtropical High Intensity Index, which are related to Xixia-Baofeng—Kaifeng; the West Pacific 850 mb Trade Wind Index and the Tropical Northern Atlantic SST Index, which are related to Zhengzhou-Xinxiang-Mengjin-Anyang; the West Wind Drift Current SST Index and the NINO B SSTA Index, which are related to Xuchang-Xihua; and the Asian Meridional Circulation Index which is related to Nanyang-Tongbai.

(2) Teleconnection factors are the main driving force of urban extreme precipitation in the study area (contribution rate of 50.3–99.8%). The contribution rate of urbanization presents a radial spatial distribution mode, that is, the overall decreasing in the central and southern part of the city and the overall increasing at the edge. The contribution of urbanization increases with the increase in the recurrence period in the areas with a high level of urbanization, maintaining the remarkable influence of urbanization indicators such as road area, built-up district area, botanical garden areas, and length of road.

(3) For most cities, the intensity and duration of extreme precipitation will increase (18.33–62.55%, 0.23–42.55%) in the future, and the growth rate will increase with the increase in recurrence period (0.86~2.14 times, 1.35~39.40 times).

Although this study established a framework for applying teleconnection factors to explore the mechanism of urban extreme precipitation under urbanization, there are still questions that need further investigation. For instance, what are the main dynamical physical processes in geopotential and wind fields leading to extreme precipitation with different return periods through the method of composite analysis? How the effects of different categories of urbanization activities on urban local climate through synthetic land surface models be simulated and quantified? Can a higher horizontal resolution further improve the prediction of such small-scale precipitation systems, like cities? Most importantly, more deep explorative work is needed to gain in-depth understanding of the associated atmospheric circulation, underlying surface modification, and precipitation processes. Nevertheless, the present results have important implications for understanding the dynamic mechanisms of urban extreme precipitation and predicting future unprecedented extreme precipitation.

**Author Contributions:** Y.Z.: Conceptualization, Methodology, Software, Writing—Original Draft. J.T.: Conceptualization, Supervision, Writing—Review and Editing. H.L.: Resources. Q.Z.: Investigation. Y.H.: Validation. W.D.: Formal analysis. All authors have read and agreed to the published version of the manuscript.

**Funding:** This study was supported by the National Natural Science Foundation of China (No. 52209037); the China postdoctoral science foundation (No. 2022M722880, 2023T160595); Project of engineering research service of Yangtze—to—Huaihe River Water Diversion (Henan section) (HNYJJH/JS/FWKY-2021002).

**Data Availability Statement:** The raw data can be obtained through a public web site, and the analyzed data used in the current study are available from the corresponding author upon reasonable request. The processed code used in this study can be accessed by contacting the corresponding author upon reasonable request.

**Acknowledgments:** The authors would like to thank the editor and the anonymous reviewers for their comments, which helped improve the quality of the paper.

**Conflicts of Interest:** The authors declare no conflict of interest.

## References

1. Wang, J.; Feng, J.; Wu, Q.; Yan, Z. Impact of anthropogenic aerosols on summer precipitation in the Beijing–Tianjin–Hebei urban agglomeration in China: Regional climate modeling using WRF-Chem. *Adv. Atmos. Sci.* **2016**, *33*, 753–766. [[CrossRef](#)]
2. Ajaaj, A.A.; Mishra, A.K.; Khan, A.A. Urban and peri-urban precipitation and air temperature trends in mega cities of the world using multiple trend analysis methods. *Theor. Appl. Climatol.* **2017**, *132*, 403–418. [[CrossRef](#)]
3. Kang, C.; Luo, Z.; Zong, W.; Hua, J. Impacts of urbanization on variations of extreme precipitation over the Yangtze River Delta. *Water* **2021**, *13*, 150. [[CrossRef](#)]

4. Li, Y.; Wang, W.; Chang, M.; Wang, X. Impacts of urbanization on extreme precipitation in the Guangdong-Hong Kong-Macau Greater Bay Area. *Urban Clim.* **2021**, *38*, 100904. [[CrossRef](#)]
5. Han, L.; Xu, Y.; Pan, G.; Deng, X.; Hu, C.; Xu, H.; Shi, H. Changing properties of precipitation extremes in the urban areas, Yangtze River Delta, China, during 1957–2013. *Nat. Hazards* **2015**, *79*, 437–454. [[CrossRef](#)]
6. Oh, S.-G.; Son, S.-W.; Min, S.-K. Possible impact of urbanization on extreme precipitation–temperature relationship in East Asian megacities. *Weather Clim. Extrem.* **2021**, *34*, 100401. [[CrossRef](#)]
7. Zhang, D.L. Rapid urbanization and more extreme rainfall events. *Sci. Bull.* **2020**, *65*, 516–518. [[CrossRef](#)]
8. Zhang, Y.; Pang, X.; Xia, J.; Shao, Q.; Yu, E.; Zhao, T.; She, D.; Sun, J.; Yu, J.; Pan, X.; et al. Regional patterns of extreme precipitation and urban signatures in metropolitan areas. *J. Geophys. Res. Atmos.* **2019**, *124*, 641–663. [[CrossRef](#)]
9. Silva, F.N.; Vega-Oliveros, D.A.; Yan, X.; Flammini, A.; Menczer, F.; Radicchi, F.; Kravitz, B.; Fortunato, S. Detecting climate teleconnections with Granger Causality. *Geophys. Res. Lett.* **2021**, *48*, e2021GL094707. [[CrossRef](#)]
10. Yoo, C.; Johnson, N.C.; Chang, C.-H.; Feldstein, S.B.; Kim, Y.-H. Subseasonal prediction of wintertime east Asian temperature based on atmospheric teleconnections. *J. Clim.* **2018**, *31*, 9351–9366. [[CrossRef](#)]
11. Zhao, S.; Zhang, J. Causal effect of the tropical Pacific sea surface temperature on the upper Colorado river basin spring precipitation. *Clim. Dyn.* **2022**, *58*, 941–959. [[CrossRef](#)]
12. Deng, Z.; Wang, Z.; Wu, X.; Lai, C.; Liu, W. Effect difference of climate change and urbanization on extreme precipitation over the Guangdong-Hong Kong-Macao Greater Bay Area. *Atmos. Res.* **2023**, *282*, 106514. [[CrossRef](#)]
13. Wei, N.; Wang, N.; Zheng, Y.; Liu, H. Contribution of climate change and urbanization to the variation of extreme precipitation in the urban agglomerations over the Loess Plateau. *Hydrol. Process.* **2022**, *36*, e14489. [[CrossRef](#)]
14. Lin, L.; Gao, T.; Luo, M.; Ge, E.; Yang, Y.; Liu, Z.; Zhao, Y.; Ning, G. Contribution of urbanization to the changes in extreme climate events in urban agglomerations across China. *Sci. Total Environ.* **2020**, *744*, 140264. [[CrossRef](#)]
15. Song, X.; Qi, J.; Zou, X.; Zhang, J.; Liu, C. Potential effects of urbanization on precipitation extremes in the Pearl River Delta region, China. *Water* **2022**, *14*, 2466. [[CrossRef](#)]
16. Zhu, X.; Zhang, Q.; Sun, P.; Singh, V.P.; Shi, P.; Song, C. Impact of urbanization on hourly precipitation in Beijing, China: Spatiotemporal patterns and causes. *Glob. Planet. Chang.* **2019**, *172*, 307–324. [[CrossRef](#)]
17. Paul, S.; Ghosh, S.; Mathew, M.; Devanand, A.; Karmakar, S.; Niyogi, D. Increased spatial variability and intensification of extreme monsoon rainfall due to urbanization. *Sci. Rep.* **2018**, *8*, 3918. [[CrossRef](#)]
18. Xu, Y.; Chen, X.; Liu, M.; Wang, J.; Zhang, F.; Cui, J.; Zhou, H. Spatial–temporal relationship study between NWP PWV and precipitation: A case study of ‘July 20’ Heavy Rainstorm in Zhengzhou. *Remote Sens.* **2022**, *14*, 3636. [[CrossRef](#)]
19. Sun, J.; Fu, S.; Wang, H.; Zhang, Y.; Chen, Y.; Su, A.; Wang, Y.; Tang, H.; Ma, R. Primary characteristics of the extreme heavy rainfall event over Henan in July 2021. *Atmos. Sci. Lett.* **2022**, *24*, e1131. [[CrossRef](#)]
20. Qin, H.; Yuan, W.; Wang, J.; Chen, Y.; Dai, P.; Sobel, A.H.; Meng, Z.; Nie, J. Climate change attribution of the 2021 Henan extreme precipitation: Impacts of convective organization. *Sci. China Earth Sci.* **2022**, *65*, 1837–1846. [[CrossRef](#)]
21. Liu, X.; Yang, M.; Wang, H.; Liu, K.; Dong, N.; Wang, H.; Zhang, L.; Fan, W. Moisture sources and atmospheric circulation associated with the record-breaking rainstorm over Zhengzhou city in July 2021. *Nat. Hazards* **2023**, *116*, 817–836. [[CrossRef](#)]
22. Zhang, G.; Mao, J.; Hua, W.; Wu, X.; Sun, R.; Yan, Z.; Liu, Y.; Wu, G. Synergistic effect of the planetary-scale disturbance, Typhoon and Meso- $\beta$ -scale convective vortex on the extremely intense rainstorm on 20 July 2021 in Zhengzhou. *Adv. Atmos. Sci.* **2023**, *40*, 428–446. [[CrossRef](#)]
23. Yin, J.; Gu, H.; Liang, X.; Yu, M.; Sun, J.; Xie, Y.; Li, F.; Wu, C. A possible dynamic mechanism for rapid production of the extreme hourly rainfall in Zhengzhou City on 20 July 2021. *J. Meteorol. Res.* **2022**, *36*, 6–25. [[CrossRef](#)]
24. Wei, P.; Xu, X.; Xue, M.; Zhang, C.; Wang, Y.; Zhao, K.; Zhou, A.; Zhang, S.; Zhu, K. On the key dynamical processes supporting the 21.7 Zhengzhou record-breaking hourly rainfall in China. *Adv. Atmos. Sci.* **2022**, *40*, 337–349. [[CrossRef](#)]
25. Deng, L.; Feng, J.; Zhao, Y.; Bao, X.; Huang, W.; Hu, H.; Duan, Y. The remote effect of binary Typhoon Infa and Cempaka on the “21.7” heavy rainfall in Henan Province, China. *J. Geophys. Res. Atmos.* **2022**, *127*, 16. [[CrossRef](#)]
26. Wang, H.; Wang, H.; Li, H.; Faisal, M.; Zhang, Y. Analysis of drainage efficiency under extreme precipitation events based on numerical simulation. *Hydrol. Process.* **2022**, *36*, e14624. [[CrossRef](#)]
27. Zhao, Y.; Son, S.W.; Back, S.Y. The critical role of the upper-level synoptic disturbance on the China Henan “21.7” extreme precipitation event. *SOLA* **2023**, *19*, 42–49. [[CrossRef](#)]
28. Efron, B.; Tibshirani, R. Bootstrap methods for standard errors, confidence intervals, and other measures of statistical accuracy. With a comment by J. A. Hartigan and a rejoinder by the authors. *Stat. Sci.* **1986**, *1*, 54–77. [[CrossRef](#)]
29. Granger, C.W.J. Investigating causal relations by econometric models and cross-spectral methods. *Econometrica* **1969**, *37*, 424–438. [[CrossRef](#)]
30. Yin, L.; Ping, F.; Mao, J.; Jin, S. Analysis on precipitation efficiency of the “21.7” Henan extremely heavy rainfall event. *Adv. Atmos. Sci.* **2022**, *40*, 374–392. [[CrossRef](#)]
31. Li, H.; Moisseev, D.; Luo, Y.; Liu, L.; Ruan, Z.; Cui, L.; Bao, X. Assessing specific differential phase (KDP)-based quantitative precipitation estimation for the record-breaking rainfall over Zhengzhou city on 20 July 2021. *Hydrol. Earth Syst. Sci.* **2023**, *27*, 1033–1046. [[CrossRef](#)]
32. Henan Province Bureau of Statistics. *Henan Statistical Yearbook*; China Statistics Press: Beijing, China, 2002–2022.
33. Mann, H.B. Nonparametric tests against trend. *Econometrica* **1945**, *13*, 245–259. [[CrossRef](#)]

34. Kendall, M. *Rank Correlation Methods*; Griffin: London, UK, 1975.
35. Pettitt, A.N. A non-parametric approach to the change-point problem. *J. R. Stat. Soc. Ser. C Appl. Stat.* **1979**, *28*, 126. [[CrossRef](#)]
36. Taylor, K.E. Summarizing multiple aspects of model performance in a single diagram. *J. Geophys. Res.* **2001**, *106*, 7183–7192. [[CrossRef](#)]

**Disclaimer/Publisher’s Note:** The statements, opinions and data contained in all publications are solely those of the individual author(s) and contributor(s) and not of MDPI and/or the editor(s). MDPI and/or the editor(s) disclaim responsibility for any injury to people or property resulting from any ideas, methods, instructions or products referred to in the content.